Regular article

Intracellular mechanics and TBX3 expression jointly dictate the spreading mode of melanoma cells in 3D environments

Ghodeejah Higgins[1], Faatiemah Higgins[2], Jade Peres[2], Dirk M Lang[2], Tamer Abdalrahman[1], Muhammad H. Zaman[3,4], Sharon Prince[2], Thomas Franz[1,5]*

[1]Biomedical Engineering Research Centre, Division of Biomedical Engineering, Department of Human Biology, University of Cape Town, Observatory, South Africa

[2]Division of Cell Biology, Department of Human Biology, University of Cape Town, Observatory, South Africa

[3]Department of Biomedical Engineering, Boston University, Boston, MA, USA

[4]Howard Hughes Medical Institute, Chevy Chase, MD, USA

[5]Bioengineering Science Research Group, Faculty of Engineering and Physical Sciences, University of Southampton, Southampton, UK

ORCID

G Higgins: 0000-0003-3576-9031

F Higgins: 0000-0002-2389-2625

J Peres: 0000-0001-8568-4840

DM Lang: 0000-0003-3901-2079

T Abdalrahman: 0000-0002-0320-811X

MH Zaman: 0000-0002-3723-5431

S Prince: 0000-0002-6975-5255

T Franz: 0000-0002-1504-3842

*Corresponding author: thomas.franz@uct.ac.za, Tel +27 21 650 1795

Department of Human Biology, Faculty of Health Sciences, University of Cape Town, Private Bag X3, Observatory 7935, South Africa

Abstract

Cell stiffness and T-box transcription factor 3 (TBX3) expression have been identified as biomarkers of melanoma metastasis in 2D environments. This study aimed to determine how mechanical and biochemical properties of melanoma cells change during cluster formation in 3D environments. Vertical growth phase (VGP) and metastatic (MET) melanoma cells were embedded in 3D collagen matrices of 2 and 4 mg/ml collagen concentrations, representing low and high matrix stiffness. Mitochondrial fluctuations, intracellular stiffness, and TBX3 expression were quantified before and during cluster formation. In isolated cells, mitochondrial fluctuations decreased and intracellular stiffness increased with increase in disease stage from VGP to MET and increase in matrix stiffness. TBX3 was overexpressed in soft matrices but diminished in stiff matrices for VGP and MET cells. Cluster formation of VGP cells was excessive in soft matrices but limited in stiff matrices, whereas for MET cells it was limited in soft and stiff matrices. In soft matrices, VGP cells did not change the intracellular properties, whereas MET cells exhibited increased mitochondrial fluctuations and decreased TBX3 expression. In stiff matrices, mitochondrial fluctuations and TBX3 expression increased in VGP and MET, and intracellular stiffness increased in VGP but decreased in MET cells. Mitochondrial activity, cellular stiffness, and TBX3 expression jointly affected cluster formation and metastasis in melanoma with contributions that vary with changes in environmental properties. This study highlights the importance of considering the biophysical and biochemical properties of the malignant cells and the extracellular environment for advancing targeted melanoma therapies.

Keywords

Cluster formation; cluster morphology; mitochondrial particle tracking microrheology; cell mechanics; T-box factor; collagen

Symbols

A	Area of a cell or cell cluster measured
$\hat{A}$	Area of cell or cell cluster predicted by a regression model
A_N	Normalized area, i.e., measured area of cell or cell cluster normalized to mean single-cell area
$\hat{A}_N$	Normalized area of cell or cell cluster, i.e., area of cell or cell cluster normalized to mean single-cell area, predicted by a regression model
A_{ROI}	Area of the region of interest in image
B	Background signal intensity in an image
I	Integrated pixel density
L_M	Length of a cell along its major axis
n	Number of biological repeats
N	Sample size
p	Indicator of statistical significance
R	Roundness of a cell or cell cluster measured
$\hat{R}$	Roundness of a cell or cell cluster predicted by a regression model
r	Mitochondrial displacement
t	Time
α	Power law coefficient
τ	Delay time, lag time in mean square displacement analysis

1. Introduction

Recent studies have shown that cancer cells continuously respond and adapt to changes in the microenvironment through altered migratory properties [1], mechanical properties [2], and gene expression [3, 4]. Some studies focused on the mechanical properties of cells in isolation, whereas other studies investigated mechanical properties of cellular aggregates. For cells in isolation, it was shown that cancer cells have enhanced biomechanical properties compared to normal cells, such as increased contractile [5] and traction force generation [1, 6, 7] and deformability [1, 8, 9]. At the cellular aggregate level, compromised rigidity of solid cancer tumours compared to normal tissue was demonstrated by measuring stiffness averaged over thousands of cells in cell spheroid models using many techniques, such as micro-tweezers [10], atomic force microscopy (AFM) [11], and cavitation rheology [12].

These studies have provided insight into the cell mechanics of various cancer types and identified mechanical properties as potential biomarkers of cancer malignancy; however, their results have not demonstrated the progressive changes in biomechanical properties as cells transition from isolated single cells to cellular aggregates. In particular, it is not understood whether isolated cells from different stages of the disease are innately endowed with sufficient mechanical properties to form tumours or if mechanical properties are adjusted in response to three-dimensional (3D) extracellular matrix (ECM) properties at distant sites of colonization.

It is increasingly being recognized that the properties of the tumour microenvironment play an essential role in the development of cancer [13]. Cells are surrounded by a rich ECM, an essential component in the microenvironment, whose chemical, physical, and mechanical properties are fundamental in orchestrating several biological processes, including tissue homeostasis, differentiation, migration and invasion [14]. The most abundant protein found in the ECM is fibrillar type I collagen [15, 16], which forms a scaffold that imparts tensile strength and stiffness to the tissue [17, 18]. It has also been reported that changes in ECM stiffness is on account of altered collagen I density [18-21]. In addition, collagen I comprises of 80-90% of the collagenase proteins in the dermis, and studies have showed that altered collagen I density affects melanoma progression *in vitro* and *in vivo* [22].

Cell-ECM interaction is mediated through mechanical machinery such as the cell's actin cytoskeleton, molecular motors, integrins, focal adhesion and GTPases [23-25], allowing cells to receive, process, and respond to biochemical and biomechanical cues from the

environment [26, 27]. The properties including composition, topography, and stiffness of tumour-derived ECM are enhanced compared to normal ECM, and crucial in administering cells with a tumorigenic genotype [19].

Although ECM mechanics and its role in guiding metastasis have received increasing attention [15, 28-31], little is known about the biomechanics of the cell-ECM relationship at distant sites of metastasis and why cells may favour specific distant organs over others. Even less is known about the cell's inherent biomechanical properties and biochemical pathways that coordinate formation of tumours in changing 3D environments, particularly at advanced stages of cancer progression. The ability of cells to form clusters is essential for tumour formation and metastasis [32].

Several assays, together with high-resolution imaging approaches, have addressed essential questions on cluster morphology, tumour growth, viability [33, 34], drug testing [4] and drug development [33, 35, 36], spheroid invasion [37-39] and cancer stem cell content [4]. Fewer studies have investigated the contribution of cell mechanics in the context of cell deformability to the detachment and invasion process. The scarcity of cell mechanics studies using cell clusters and spheroids is, in part, due to technical challenges involved in quantifying cell mechanics in 3D environments, in particularly the detachment and invasion process in a live-cell 3D realistic model. Microrheological methods, in particular those facilitating the tracking of endogenous nano-particles such as mitochondria inside the cells, can offer non-invasive techniques to passively probe cell mechanics without introducing any cellular or matrix deformation [2]. Furthermore, local responses are probed, which makes it convenient in investigating cell mechanics in complex environments in which single and collective cell behaviour may co-exist.

A central therapeutic goal has been to target key molecular regulators of advanced-stage cancers. The AKT3 signalling pathway plays a critical role in melanoma formation and invasion and we have reported that TBX3 is a key substrate of AKT3 in melanomagenesis [40]. We have shown that AKT3 phosphorylates TBX3 at S720 and this promotes TBX3 protein stability, nuclear localization, transcriptional repression of E-cadherin, and its role in cell migration and invasion. We have also previously reported that TBX3 levels are high in VGP and metastatic melanoma and that depleting TBX3 in these cells inhibits their ability to form tumours [41]. Consistent with these findings, when TBX3 alone was overexpressed in RGP non-malignant melanoma cells it was sufficient to promote tumour formation and invasion [42].

Although it is known that TBX3 is overexpressed in several cancers [43], knowledge of mechanical mediators of TBX3 regulation such as matrix rigidity is very limited. Research on TBX3 has been conducted predominantly in 2D *in vitro* conditions and in *in vivo* animal models. However, cells in 2D environments do not fully depict physiologically cell-cell and cell-matrix interactions [44]. *In vivo* models mimic complex cell-cell and cell-matrix interaction better but exhibit spatially complex microenvironments whose environmental cues, as ECM properties, are challenging to control [45].

Considering that TBX3 promotes tumour formation in melanoma cancers, and the current understanding that tumour formation is dependent on the mechanical environment, the aim of the current study was two-fold, namely to determine how (a) mechanical mediators, such as cell stiffness and matrix rigidity, impact cluster formation of advanced melanoma cells and (b) TBX3 levels change in melanoma cells during cluster formation in 3D *in vitro* collagen matrices of varying rigidity.

2. Materials and methods

2.1. Cell seeding

Advanced human melanoma cell lines, ME1402 vertical growth phase (VGP) and WM1158 metastatic (MET), were cultured using RPMI 1640 media (Life Technologies), supplemented with 10% foetal bovine serum (FBS) and 1% penicillin-streptomycin. Before passaging or experimentation, cells were grown to near-confluence in 25 cm^2 tissue flasks (Costar, Corning Life Science, Acton, MA) at 37°C and 5% CO_2. Media was replaced every 3-4 days.

2.2. Collagen embedding

Single cells were embedded in 2 and 4 mg/ml collagen solutions. Collagen solutions comprised Type I Rat Tail Collagen (BD Biosciences, stock solution of 8.21 mg/ml) and neutralizing solution (100 mM HEPES in 2X PBS with pH 7.3) in a 1:1 ratio, diluted with 1XPBS to final concentrations of 2 and 4 mg/ml collagen. For each condition, 50 µl of unpolymerized collagen solution was placed on glass-bottom dishes and incubated at 37°C and 5% CO_2 for 1 hr. After gels polymerized, 500 µl media were added to the wells.

2.3. Morphological assessment

Cellular morphology was assessed on Day 1 for isolated cells and Days 4, 7 and 10 for cell clusters. Media was replaced every three days. Phase-contrast images of cells were acquired on a Zeiss LSM 880 with Airyscan confocal microscope (Carl Zeiss Microimaging, Germany) with a 63x 1.4 oil immersion objective and an electron-multiplying CCD camera (Hamamatsu Photonics, Hamamatsu, Japan). Cells or cell clusters located near the middle of the gel were imaged. At least 28 images were acquired per condition from three repeat experiments (n = 4).

Images were post-processed and morphometrically assessed using Image J [46] to quantify cell area A and roundness $R = 4A/(\pi \cdot L_M^2)$, where L_M refers to the length of the cell along the major axis. Higher values of R represented rounder shapes. Isolated cells and cell clusters were considered round for $R \geq 0.80$ and elongated for $R < 0.80$.

2.4. Mitochondrial particle tracking microrheology

Microrheology experiments were conducted on isolated cells on Day 1 and cell clusters on Day 7. Mitochondria were fluorescently labelled 1 hr before experimentation by incubating cells with 350 nM Mitotracker Green solution (Life Technologies, Carlsbad, CA) added to RPMI 1640 media. Cells and cell clusters near the middle of the collagen gel were imaged in time-lapse mode (50 ms per frame for 120 s) to capture mitochondrial fluctuations. Time-lapse images were collected with a Zeiss LSM 880 with Airyscan confocal microscope (Carl Zeiss Microimaging, Germany) with 63x 1.4 oil immersion objective and an electron-multiplying CCD camera (Hamamatsu Photonics, Hamamatsu, Japan). Experiments were repeated at least once (n = 2), each time assessing at least 24 isolated cells per condition and 16 cell clusters. At least four outer cells per cluster were assessed.

For analysis, time-lapse images of cells with at least 60 mitochondria and each mitochondrion visible for at least 80% of the total acquisition time were used. Mitochondrial particle trajectories were constructed in TrackMate [47] and converted to the mean square displacement (MSD) using @msdanalyzer [48] in MATLAB (The MathWorks, Natick, MA).

The ensemble-averaged MSD $\langle \Delta r^2 (\tau)_{xy} \rangle$ was calculated according to:

$$\langle \Delta r^2(\tau)_{xy} \rangle = \langle [x(t+\tau) - x(t)] + [y(t+\tau) - y(t)] \rangle^2. \quad (1)$$

Here, τ is the delay time between the first and last image frame used for the analysis, and x(t) and y(t) are the spatial coordinates of mitochondrial particle positions at time t.

For viscoelastic materials, the MSD scales nonlinearly with τ according to a power-law relationship, $\langle \Delta r^2 (\tau)_{xy} \rangle \sim \tau^{\alpha}$. The MSD-dependant power-law coefficient α was determined as a measure of intracellular fluidity (deformability):

$$\alpha = \frac{\partial \ln\langle \Delta r^2(\tau) \rangle}{\partial \ln(\tau)} \,. \tag{2}$$

2.5. Immunofluorescent quantification of TBX3 and F-actin

Cells were stained for either TBX3 on Day 1 and 7 or F-actin on Day 7 as previously described [49]. In brief, cells were gently washed with PBS and fixed with 4% paraformaldehyde in PBS at room temperature for 20 min. Cells were washed thrice with PBS and permeabilized with 0.2% Triton X-100 in PBS at room temperature for 10 min. Cells were blocked in 5% sheep serum in PBS for 1 hr at room temperature and washed once with PBS/Tween. For TBX3 staining, cells on Day 1 and cell clusters on Day 7 were incubated overnight at 4°C with rabbit polyclonal anti-TBX3 antibody (Zymed 42-4800, Zymed Laboratories) at a 1:50 dilution in 5% sheep serum. Next, cells were washed thrice with PBS/Tween, incubated with Cy3 donkey anti-rabbit IgG (Jackson ImmunoResearch Laboratories, Inc., USA) at a dilution of 1:1000 for 60 min and washed thrice more with PBS/Tween. For actin staining, cell clusters on Day 7 were incubated overnight with 100 nM Acti-stain™ 488 Phalloidin (Cat. #PHDG1, Cytoskeleton Inc., USA) and washed thrice with PBS. Nuclei were counterstained with 1 µg/ml Hoechst (Sigma, USA) for 10 min and finally washed thrice in PBS before imaging.

A series of confocal cross-sectional images with a constant step size of 0.5 µm (z-stack) per cell cluster was acquired (Zeiss LSM 880 AiryScan microscope, 63x 1.4 oil immersion objective) and converted to a single image employing the maximum intensity projection (MIP) (ZEN lite black edition, Zeiss, Germany). The fluorescence in MIP images was quantified as the corrected total cell fluorescence CTCF = $I - A_{\mathrm{ROI}} \cdot b$, where I is the integrated pixel density (sum of all pixels) of the region of interest for fluorescence quantification, A_{ROI} is the area of the region of interest, and b is the mean fluorescence of the background in the region of interest [50].

The schedule of the experimental activities and assessments is summarised in the supplemental Table S2.

2.6. Statistical analysis

The normality of data was evaluated using the Shapiro-Wilk test. Data were reported as mean ± standard deviation in the text and mean and standard error of the mean (SEM) in graphs. All evaluations used $p < .05$ for statistical significance unless otherwise stated, e.g., for multiple comparisons.

Regression models determined whether disease stage, collagen matrix concentration and time point of the experiments were predictors of area and roundness of isolated cells and cell clusters. For area measurements, multiple linear regression models were derived to predict the cluster size as either absolute area, $\hat{A}$, or as area normalized to the mean single-cell area, $\hat{A}_N$. Beta regression models were employed to predict the roundness $\hat{R}$.

Microrheology, TBX3 and F-actin data were assessed with multi-factorial ANOVA for significant main effects and two- or three-way interactions among variables. Significant interactions were further assessed with linearly independent pairwise comparisons among estimated marginal means.

Statistica for Windows (Version 13.5, TIBCO Software Inc., Palo Alto, CA) was used for regression model analysis, and SPSS for Windows (Version 25, IBM Corp., Armonk, NY) was used for all other analyses.

3. Results

3.1. Morphology

3.1.1. VGP isolated cells and cell clusters were larger than MET counterparts

Morphology measurements were obtained from 28 images from three repeat experiments (n = 4).

For absolute cell area, the advanced disease stage (MET versus VGP) exhibited a marked decrease of the predicted area $\hat{A}$ on Day 1 and Day 4 ($p < .001$ and $p = .001$, respectively) and a slight decrease of $\hat{A}$ on Day 7 and Day 10 ($p = .254$ and $p = .168$, respectively) , Figure 1a. Increased collagen concentration from 2 to 4 mg/ml correlated with a decrease of $\hat{A}$ of cells on Day 1 ($p = .004$). For cell clusters, increased collagen concentration correlated with a decrease of $\hat{A}$ on Day 4 and 7 ($p = .435$ and $p = .512$, respectively), although this was not significant, and had no effect on $\hat{A}$ on Day 10 ($p = .740$).

For normalized cluster area, advanced disease stage correlated with a decrease in $\hat{A}_N$ on Day 4 and Day 7 ($p < .001$ and $p =.001$, respectively) but did not alter $\hat{A}_{\mathrm{N}}$ on Day 10 ($p = .222$). Increased collagen concentration correlated with a decrease in $\hat{A}_{\mathrm{N}}$ on Day 4 and Day 7 ($p = .154$ and $p = .616$, respectively), although not significant, and did not alter $\hat{A}_{\mathrm{N}}$ on Day 10 ($p = .990$).

Finally, increased time points from Day 1 to Day 4, 7 and 10, respectively, correlated with an increase of $\hat{A}$ and $\hat{A}_{\mathrm{N}}$ ($p < .001$ for all cases), indicating cluster growth.

Pairwise comparisons indicated that the absolute area was larger for VGP cells than for MET cells at each time point and for both collagen concentrations ($p < .001$). However, when normalized, VGP clusters were larger than MET clusters on Days 4 and 7 in 2 mg/ml ($p < .001$ for both cases) and in 4 mg/ml collagen ($p < .001$ and $p = .002$, respectively). For Day 10, VGP and MET clusters had similar normalized area in 2 and 4 mg/ml collagen ($p = .085$ and $p = .008$, respectively). To account for multiple comparison testing, Bonferroni correction led to significance at $p < .006$.

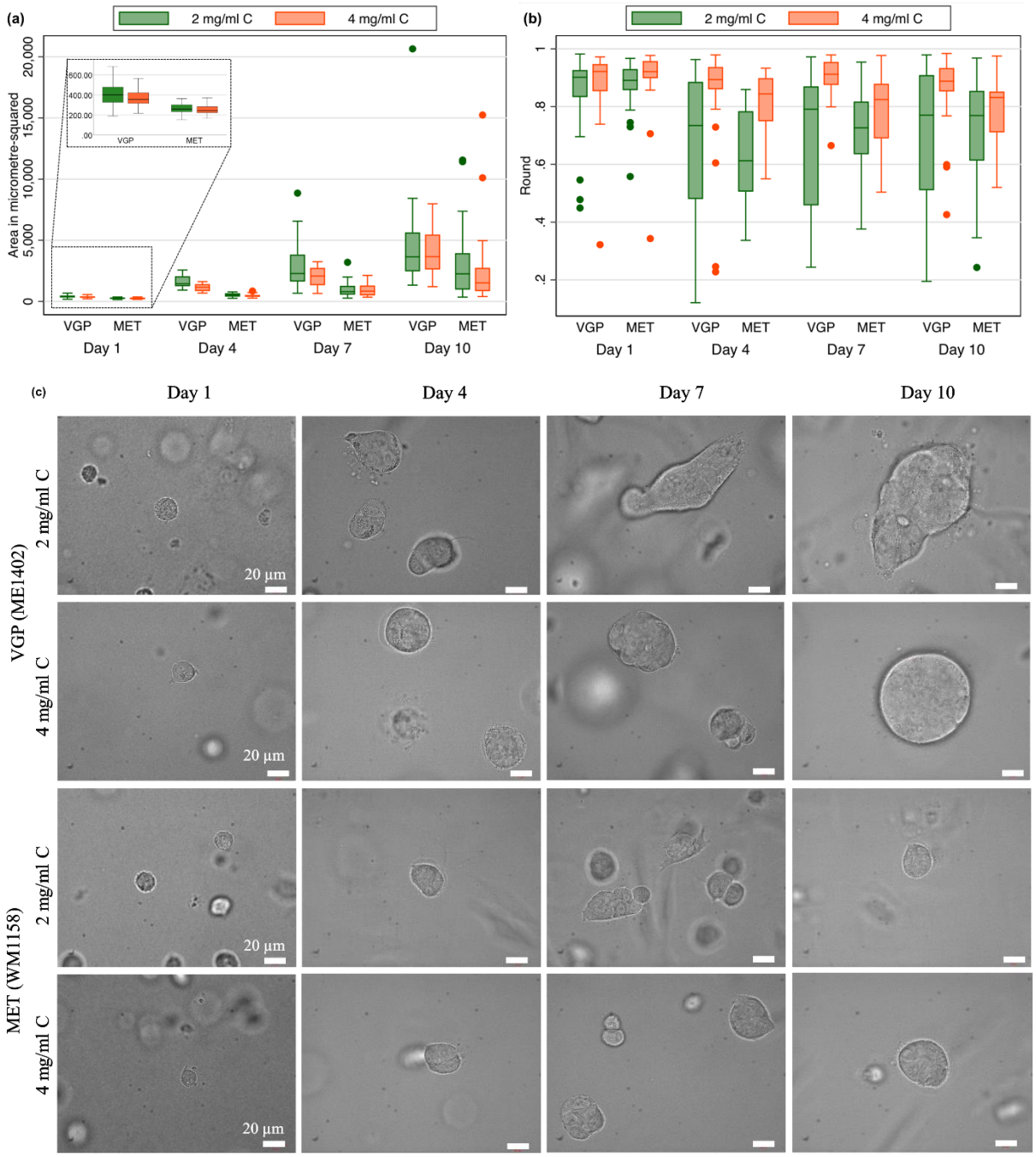

Figure 1: Morphology of VGP and MET cells over 10 days. (a) VGP cells exhibited a larger area A than MET cells ($p < .001$) for all time points and collagen concentrations. (b) Isolated VGP and MET cells on Day 1 were round ($R \geq 0.8$) irrespective of the collagen concentration of the matrix. VGP and MET cell clusters were mostly elongated ($R < 0.8$) for 2 mg/ml collagen concentration (C) and round for 4 mg/ml collagen concentration. (c) Representative confocal brightfield images of VGP and MET cells in 2 and 4 mg/ml collagen concentration at Days 1, 4, 7 and 10. (All images 63x magnification and scale bars represent 20 µm.)

3.1.2. Roundness of cell clusters increased with increased collagen concentration

Isolated cells and cell clusters were considered round for median roundness $R \geq 0.80$ and elongated for $R < 0.80$ (Figure 1b). Isolated VGP and MET cells (Day 1) were predominantly round, regardless of collagen concentration, with some notably elongated cells (outliers). In comparison, VGP and MET cell clusters were mostly elongated in 2 mg/ml collagen and round in 4 mg/ml collagen (Figure 2).

A beta regression model showed that an increase in time from Day 1 to 4, 7 and 10, respectively ($p < .001$, $p = .002$, and $p = .006$, respectively), correlated with a decrease in $\hat{R}$. In contrast, an increase in collagen concentration from 2 to 4 mg/ml correlated with an increase in $\hat{R}$ on Day 4 and 7 ($p = .045$ and $p = .019$, respectively) but did not contribute to changes in $\hat{R}$ on Day 1 and Day 10 ($p = .327$ and $p = .132$, respectively).

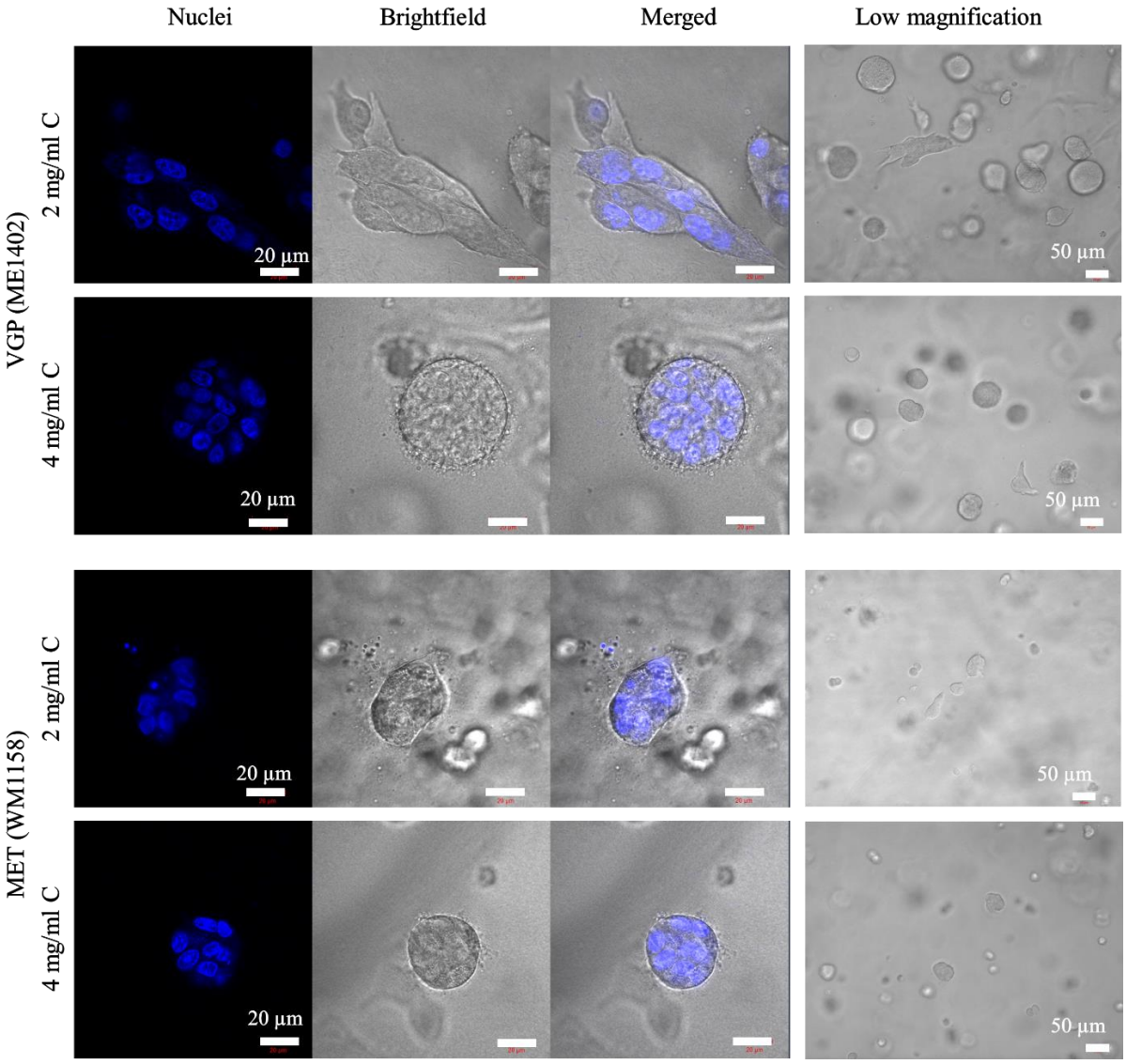

Figure 2: Confocal images (2D confocal plane) of VGP and MET clusters after 7 days in 2

and 4 mg/ml collagen (C) matrices. Each panel presents fluorescently labelled nuclei (blue), brightfield image and merged image, and low a magnification brightfield image showing multiple clusters (from left to right). In 2 mg/ml C, the elongated shape was more defined for VGP clusters than MET clusters. Increased collagen concentration compacted and rounded the cell clusters. (Nuclei, brightfield and merged images 63x magnification, scale bars represent 20 µm. Low magnification images 20x magnification, scale bars represent 50 µm).

3.2. Structural properties of cell clusters

The actin cytoskeleton is vital in controlling global cell morphology and structure [51]. Cell clusters on Day 7 were processed for immunofluorescence to detect F-actin and visualized by confocal microscopy.

3.2.1. Elongated VGP clusters formed supracellular features, and large VGP clusters merged from smaller clusters

Elongated VGP clusters were categorized as sharp- or blunt-edged in 2 mg/ml collagen (Figure 3a, b). Sharp-edged clusters comprised mostly large, elongated cells that formed supracellular features, such as supracellular protrusive fronts and retracting tails (Figure 3a, blue arrows). Elongated clusters with a blunt edge showed no supracellular protrusions; however, microspikes were present. More importantly, 2D planes showed clear borders outlining at least two clusters that had merged into one cluster (see dashed lines in Figure 3b).

Interestingly, actin visualization demonstrated merged VGP clusters in 2 mg/ml collagen (Figure 3c). Thick actin bundles (white arrow) were apparent at the interface of merged clusters.

Round VGP clusters exhibited similar actin-filled pseudopodia in 2 and 4 mg/ml collagen (Figure 3c, d). Several filopodia and microspikes emanated from cells at the cluster surface. Many clusters in 4 mg/ml collagen consisted of a single large and round cell ($R > 0.90$) with a thick actin cortex in the cluster's interior. This cell was more than twice the size of neighbouring cells.

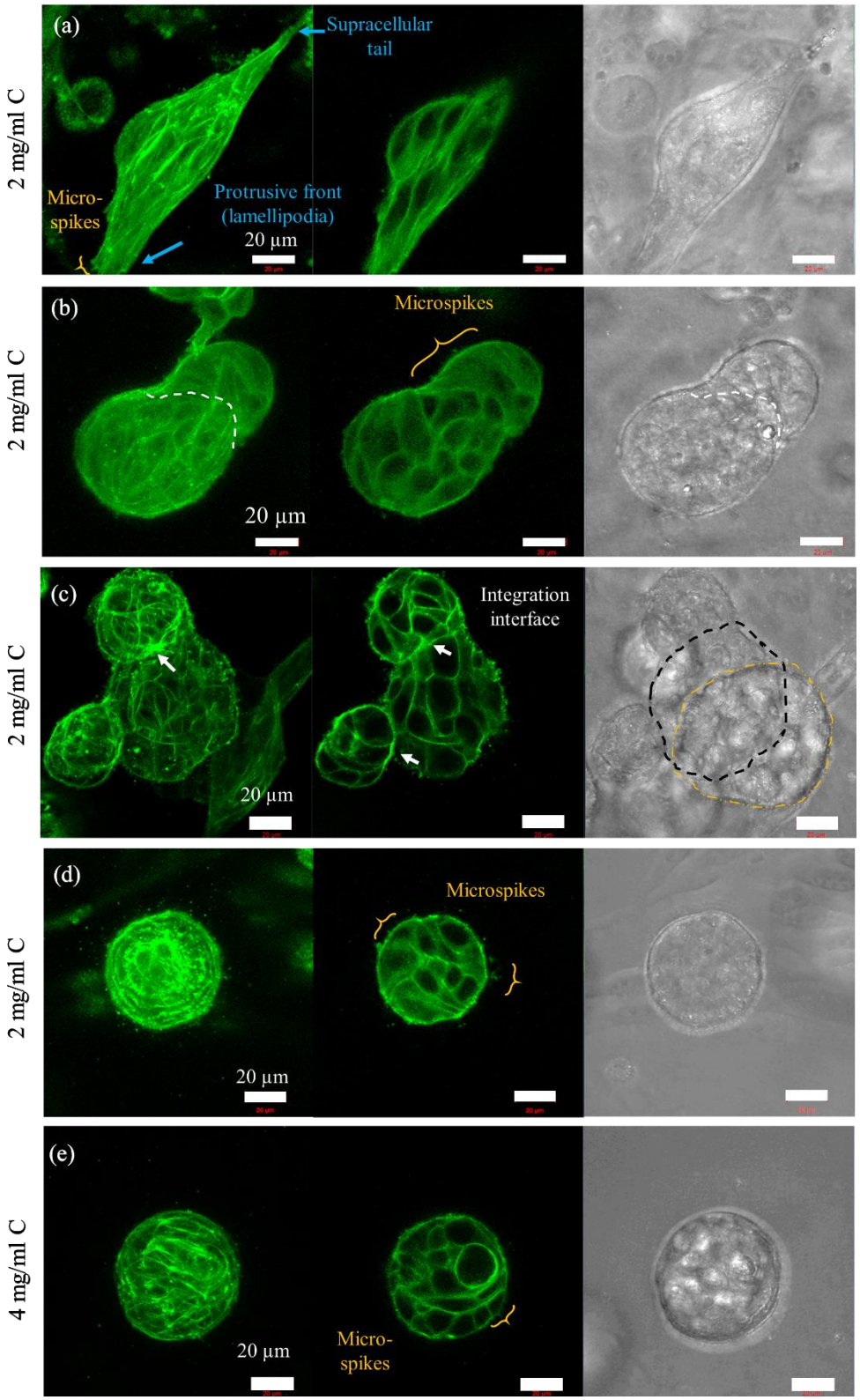

Figure 3: Confocal images of elongated (a, b), merged (c), and rounded (d, e) VGP cell clusters after 7 days in 2 and 4 mg/ml collagen (C) matrices. Each panel shows the mean intensity projection (MIP) of multiple fluorescently labelled F-actin (green) of confocal image stacks (left), F-actin of the mid-2D plane (middle) and MIP of brightfield confocal image stacks (right). All images at 63x magnification; scale bar represents 20 µm. (a,b) Elongated VGP clusters were distinguished by sharp or blunt edges in 2 mg/ml

collagen. Sharp-edged cluster (a) exhibiting supracellular edge features, i.e. protrusive front and retracting tail (blue arrows and text). Microspikes (gold bracket) were visible on the protrusions. Blunt-edge cluster (b) merged from two smaller clusters (white dashed line shows the merging site).
(c) Merged clusters resulted from two or more cell clusters that migrated towards each other and merged in 2 mg/ml collagen. The interface of merged clusters (white arrows) consisted of thick F-actin bundles in fluorescence images. The merged interface in (c) is outlined (black dashed curve) in brightfield images to distinguish it from the separate cluster not part of the merged cluster. Yellow dashed curve outlines a separate cluster that appeared in the field of view but is not attached to the merged cluster.
(d, e) For round VGP clusters in 2 mg/ml collagen (d) and 4 mg/ml collagen (e), pseudopodia were primarily in the form of finger-like protrusions. Most of the round clusters in 4 mg/ml C contained a large cell towards the cluster interior.

3.2.2. MET clusters exhibited several types of pseudopodia in 2 mg/ml collagen but were only in the form of filopodia in 4 mg/ml collagen

MET clusters invaded the 2 mg/ml collagen environment as either loose (i.e. non-adherent) or compact cell groups. In loose MET clusters, the first cell in the cluster, the leader cell, had a planar protrusive front. All cells had a retracting tail (see blue arrows in Figure 4a). Each cell within the cluster exhibited a thick actin cortex, and filopodia and microspikes emanating from the cell membrane. The thickest actin cortex and the most prominent filopodia and microspikes were observed in the leader cell (Figure 4a).

Compact MET clusters were either elongated or round in 2 mg/ml collagen, as in VGP clusters, and mostly round in 4 mg/ml collagen. Elongated compact clusters formed supracellular planar protrusive front and retracting tails (Figure 4b). Round MET clusters extended varying pseudopodia, with a complexity that depended on matrix rigidity. In 2 mg/ml collagen, round MET clusters exhibited branching filamentous pseudopodal networks, known as reticulopodia, and several filopodia (Figure 4c). In 4 mg/ml collagen, long filopodia and short microspikes were present (Figure 4d).

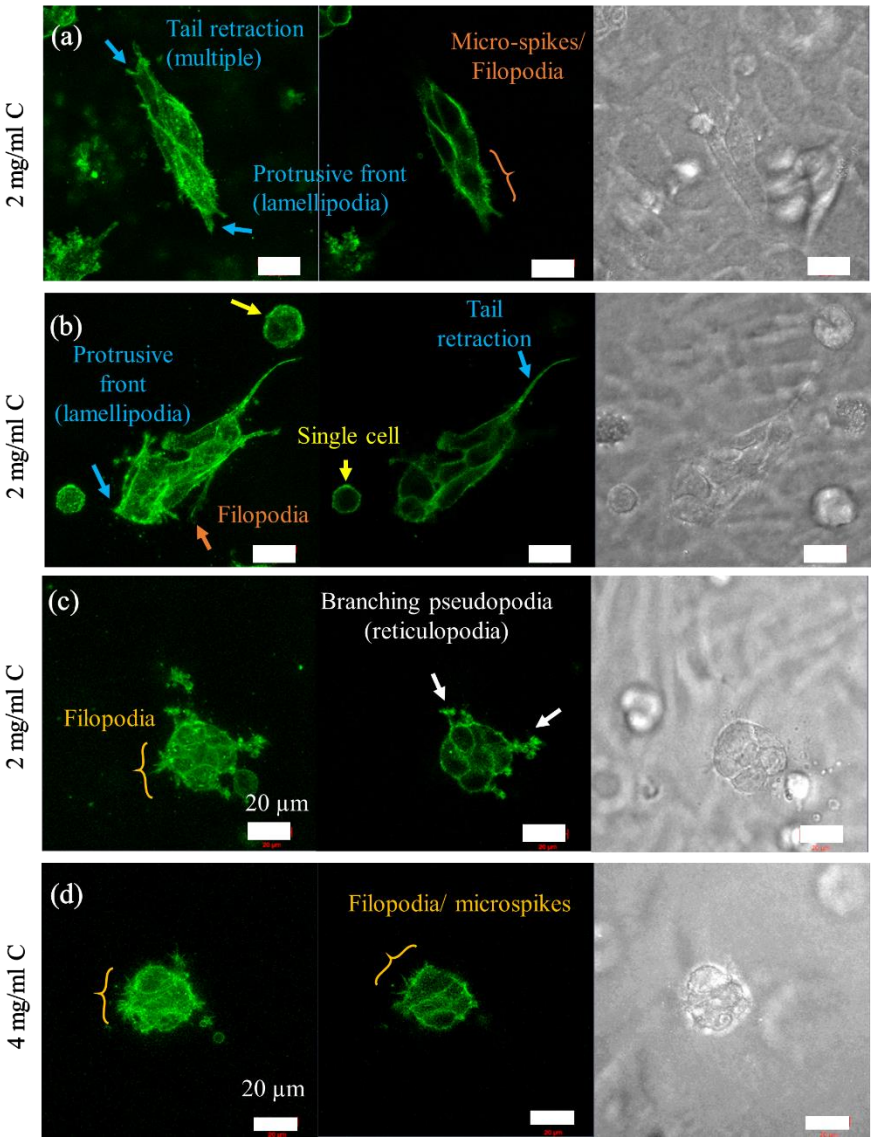

Figure 4: Confocal images of elongated (a, b) and round (c, d) MET cell clusters after 7 days in 2 and 4 mg/ml collagen (C) matrices. Each panel shows the mean intensity projection (MIP) of multiple fluorescently labelled F-actin (green) of confocal image stacks (left), F-actin of the mid-2D plane (middle) and MIP of brightfield confocal image stacks (right). All images at 63x magnification; scale bar represents 20 µm.
(a, b) Elongated MET clusters were either loose or compact in 2 mg/ml collagen. (a) Loose clusters comprised cells aligned with each other. Each cell in the cluster featured one retracting tail (blue arrow and label). (b) Compact elongated clusters emerged as supracellular units with a protrusive front and retracting tails (blue arrows and label). Single cells in the cluster's vicinity were polarised as indicated by the focalized F-actin in the cortex (yellow arrow and label). Slender filopodia and microspikes are indicated with orange arrows, respectively.
(c, d) Rounded MET clusters exhibited complex branching pseudopodia (white arrows) and filopodia (orange bracket) in 2 mg/ml collagen (c) compared to simple filopodia and microspikes in 4 mg/ml collagen (d).

3.3. Mechanical properties

Mitochondrial particle tracking experiments were conducted to investigate the intracellular mechanics of isolated cells and cell clusters. Mitochondrial fluctuations were traced and used to calculate the mean squared displacement (MSD) and power-law coefficient α.

Low MSD values, based on small mitochondrial fluctuations, correspond to inhibited particle displacement and indicate stiffer, solid materials. High MSD values, representing large mitochondrial fluctuations, indicate a greater particle motility and a softer, more fluid-like material. The MSD was determined for different delay times τ, i.e. the period between the first and the last image frame used for the analysis. Particles may displace small amounts due to random forces from the surrounding medium's thermal energy during short delay times, or displace large amounts due to active, motor-driven processes at large delay times [2, 44, 52].

The power-law coefficient α (representing the slope of the logarithmic MSD-delay time curve) characterizes the power-law delay time dependence and helps classifying the motion of the tracer particles. An α close to 1 corresponds to diffusive motion such as thermal fluctuations in a Newtonian fluid whereas an α close to 0 indicates constrained, sub-diffusive motion such as thermal fluctuations in an elastic material [44, 53]. Mitochondrial particles typically experience considerable intracellular traffic and therefore undergo constrained, sub-diffusive particle fluctuation with $0 < \alpha < 1$, which can be further classified into strong ($0 < \alpha < 0.3$) or weak ($0.7 < \alpha < 1$) sub-diffusive motion.

Lower and flat MSD-τ curves (e.g. Figure 5 b-d) indicate solid-like intracellular behaviour whereas higher and increasingly sloped curves indicate more fluid-like, intracellular motor-driven mechanics.

3.3.1. VGP were more deformable than MET isolated cells

For isolated cells, the MSD and power-law coefficient α were larger for VGP cells than for MET cells in 2 and 4 mg/ml collagen matrices at short (MSD at $\tau = 0.05$ s and α at $\tau = 1$ s), intermediate (MSD and α at $\tau = 3$ s), and large delay times (MSD and α at $\tau = 5$ s), see Figure 5(a) and Table S1.

The MSD and α of isolated VGP cells were similar in 2 and 4 mg/ml collagen matrices for all delay times τ. For MET cells, the MSD of cells in 4 mg/ml collagen compared to cells in 2 mg/ml collagen increased with delay times, with statistical significance indicated for $\tau \geq 5$ s. α of MET cells decreased for increased collagen concentration for all delay times (Figure 5a).

A decrease in MSD and α, respectively, indicated that mitochondrial fluctuations were impeded, and cells changed from fluid- to solid-like behaviour. The more advanced MET disease stage exhibited decreased mitochondrial fluctuations and increased cell stiffness of isolated cells in 2 and 4 mg/ml collagen (Figure 5b - e). Increased collagen concentration correlated with decreased mitochondrial fluctuations and increased cell stiffness for MET but not VGP cells.

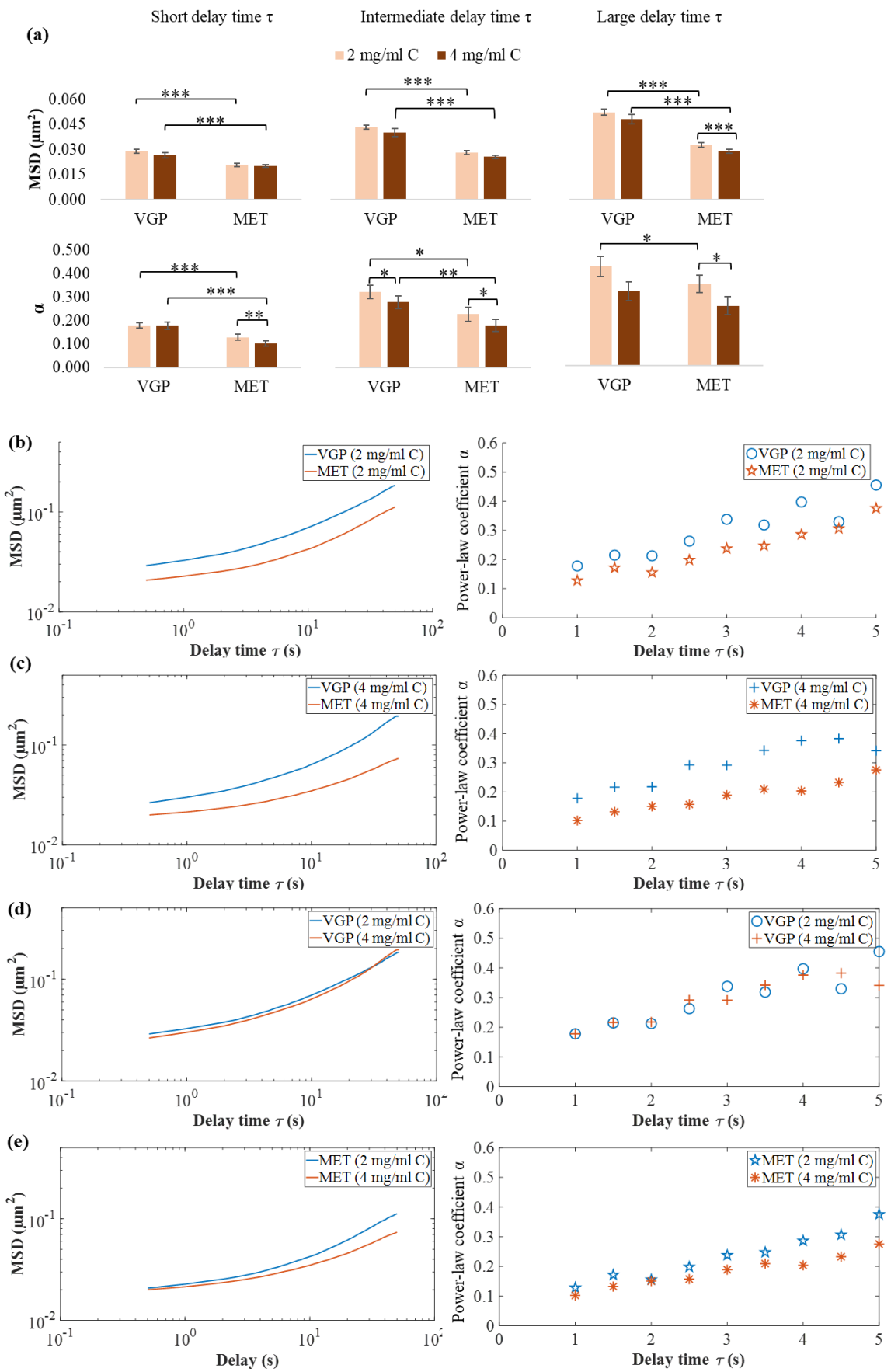

Figure 5: MSD and power-law coefficient α of VGP and MET ***isolated cells*** *(i.e. at Day 1) in*

matrices with 2 and 4 mg/ml collagen concentration (C). a) Comparison of disease stage and collagen concentration at short (MSD: $\tau = 0.05$ s, α: $\tau = 1$ s), intermediate (MSD and α: $\tau = 3$ s) and long delay time (MSD and α: $\tau = 5$ s). b, c) Comparison of different disease stages for the same collagen concentration. MET cells had lower MSD and α than VGP cells in 2 mg/ml C (b) and 4 mg/ml C (c). d, e) Comparison of the same disease stage for different collagen concentrations. MSD and α of VGP cells were similar in 2 and 4 mg/ml C (d), whereas MSD and α of MET cells were higher in 2 than 4 mg/ml C (e). Higher MSD and α indicate increased mitochondrial fluctuations and decreased cell stiffness. Error bars omitted for clarity.

3.3.2. VGP and MET cell clusters exhibited similar deformability

The MSD of cell clusters was larger at the MET than the VGP disease stage in 2 mg/ml collagen for short, intermediate, and large delay times. However, the α of VGP and MET clusters were similar. In 4 mg/ml collagen, the MSD and α of VGP and MET clusters were similar.

For VGP clusters, the MSD increased for all τ, whereas α decreased, with increased collagen concentration. A significant reduction in α was detected for $\tau \geq 3$s. A reduction in α indicated that increased collagen concentration stiffened or induced a solid-like response in VGP cells. For the MET stage, the MSD and α of clusters in 2 and 4 mg/ml collagen were similar (Figure 6a).

The advanced disease stage of cell clusters was reflected in increased mitochondrial fluctuations in 2 mg/ml collagen but did not change in 4 mg/ml collagen. The cell stiffness of MET and VGP clusters was similar both in 2 mg/ml and 4 mg/ml collagen (Figure 6b - e). Increased collagen concentration increased mitochondrial fluctuations and cell stiffness in VGP clusters but not in MET clusters.

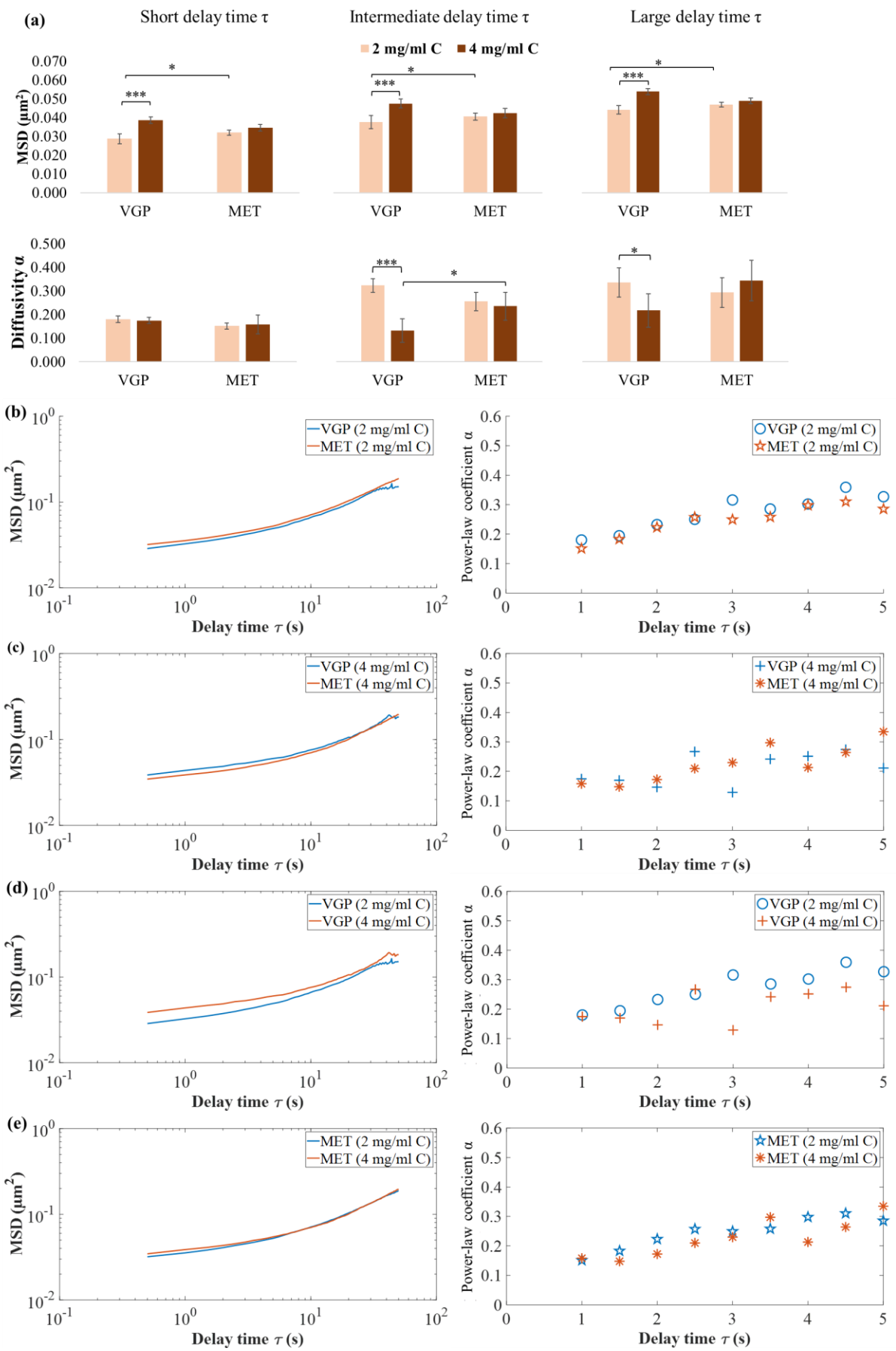
(a)
Short delay time τ
Intermediate delay time τ
Large delay time τ
2 mg/ml C
4 mg/ml C
MSD (μm²)
Diffusivity α
VGP
MET
(b)
VGP (2 mg/ml C)
MET (2 mg/ml C)
(c)
VGP (4 mg/ml C)
MET (4 mg/ml C)
(d)
VGP (2 mg/ml C)
VGP (4 mg/ml C)
(e)
MET (2 mg/ml C)
MET (4 mg/ml C)
Power-law coefficient α
Delay time τ (s)

Figure 6: MSD and power-law coefficient α of VGP and MET ***cell clusters*** *(Day 7) in matrices with 2 and 4 mg/ml collagen concentration (C). a) disease stage and collagen concentration at short (MSD: τ = 0.05 s, α: τ = 1 s), intermediate (MSD and α: τ = 3 s) and long delay time (MSD and α: τ = 5 s). b, c) Comparison of different disease stages for the same collagen concentration. The MSD and power-law coefficient α of VGP clusters were similar to that of MET clusters in 2 mg/ml C (b) and 4 mg/ml C (c). d, e) Comparison of the same disease stage for different collagen concentrations. For VGP clusters, the MSD was smaller, and α was larger in 2 mg/ml C than in 4 mg/ml C (d). MET clusters did not exhibit differences in MSD and α in 2 and 4 mg/ml C (e).*

3.3.3. Mitochondrial fluctuations increased with cluster formation, except for VGP cells in soft matrices

Active processes such as molecular motor activity, prevalent during larger delay times [2], typically drive mitochondrial fluctuations into diffusive regimes [52]. Our results did not indicate significant effects of such active processes for the selected delay times since the mitochondrial fluctuations of cells before and after cluster formation were strongly sub-diffusive ($\alpha \leq 0.3$).

Comparison of MSD data during the onset of cluster formation in 2 mg/ml collagen revealed that the MSD and α of VGP clusters (Day 7) were similar to that of isolated VGP cells (Day 1) for all τ (Figure 7a). For MET cells, the MSD increased, but α did not change while isolated cells evolved into cell clusters (Figure 7b).

In 4 mg/ml collagen, the MSD was larger for VGP clusters than for isolated VGP cells for $\tau <$ 10 s. However, the MSD converged for the largest delay times considered. The power-law coefficient α of VGP clusters were smaller than that of isolated VGP cells for $\tau > 1$ s (Figure 7c). The MSD of MET cells increased with cluster formation, but unlike VGP cells, diverged for the largest delay times. The power-law coefficient α of MET clusters was larger than that of isolated MET cells for all τ (Figure 7d). Decreased α in VGP and increased α in MET cells indicated that VGP cells stiffened, whereas MET cells softened during cluster formation.

In summary, the onset of cluster formation in 2 mg/ml collagen led to increased mitochondrial fluctuations of MET cells but did not affect VGP cells. Further, similar α indicated that cells were equally stiff before and after cluster formation. In contrast, cluster formation in 4 mg/ml collagen generally led to increased mitochondrial fluctuations of VGP and MET cells. However, the cell stiffness of VGP cells increased, whereas that of MET cells decreased (Figure 7).

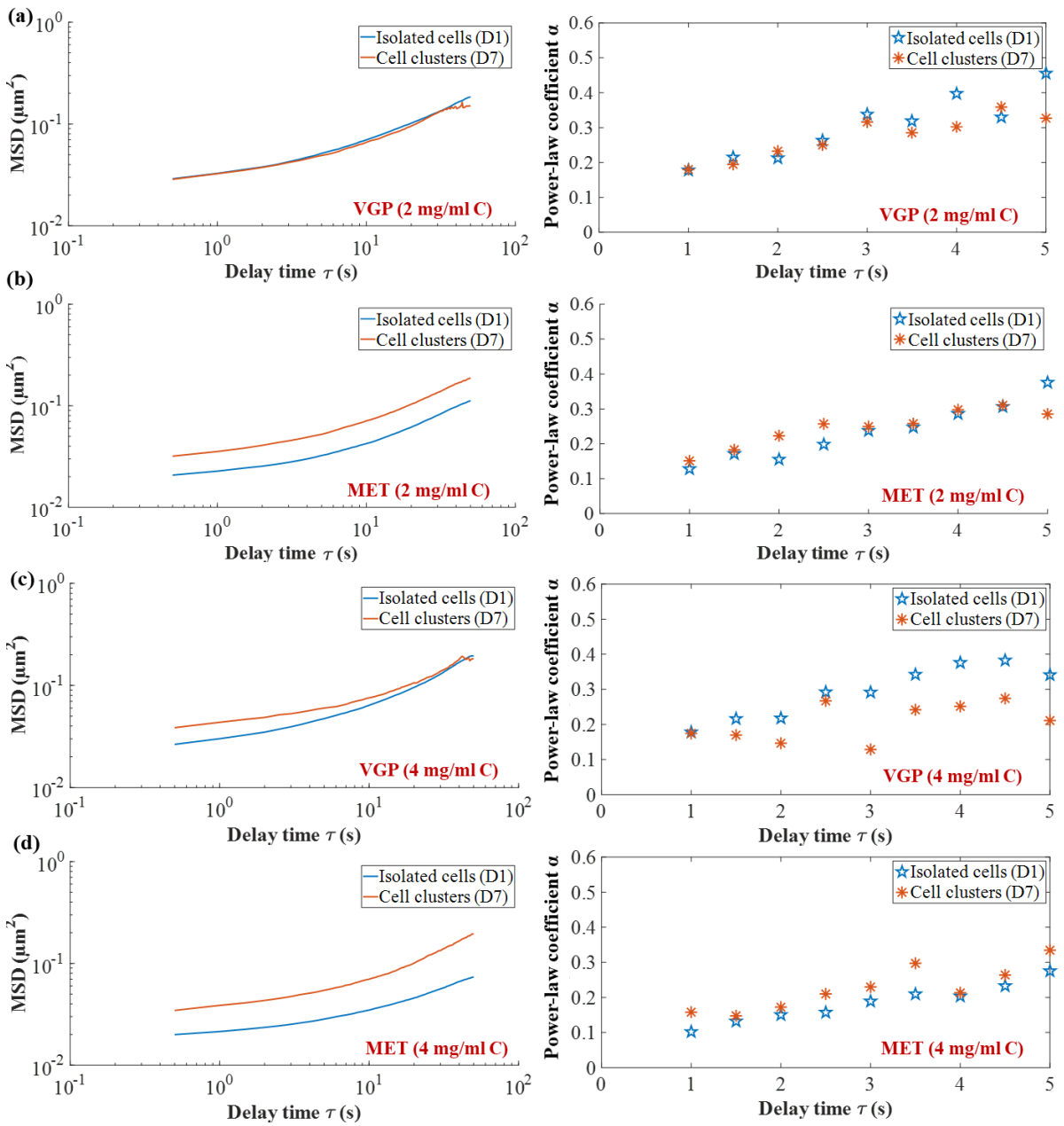

Figure 7: MSD and power-law coefficient α of ***isolated cells*** *and* ***cell clusters*** *in 2 mg/ml (a, b) and 4 mg/ml collagen (C) matrices (c, d) to illustrate the effect of cluster formation on intracellular microrheological properties. In 2 mg/ml collagen, the MSD and α of VGP isolated cells were similar to those of VGP cell clusters (a). For MET cells, the MSD was larger for clusters than for isolated cells, whereas α did not change (b). In 4 mg/ml collagen, VGP clusters exhibited larger MSD and α than isolated VGP cells (c). For MET cells, MSD substantially increased, but α decreased during cluster formation (d). (D1 = Day 1 and D7 = Day 7. Error bars omitted for clarity.)*

3.4. Expression of oncogenic factor TBX3

TBX3 belongs to the T-box family of transcription factors with fundamental roles in development, cell fate and tissue homeostasis [54]. However, overexpression of TBX3 has

been implicated in several cancers where it is crucial for cell migration and tumour formation [43].

For immunofluorescence assessment, TBX3 of at least nine isolated cells (at Day 1) and nine cell clusters (at Day 7), for n = 2 experiments, were stained, and cell nuclei were counterstained (Figure 8). Nuclear TBX3 was measured.

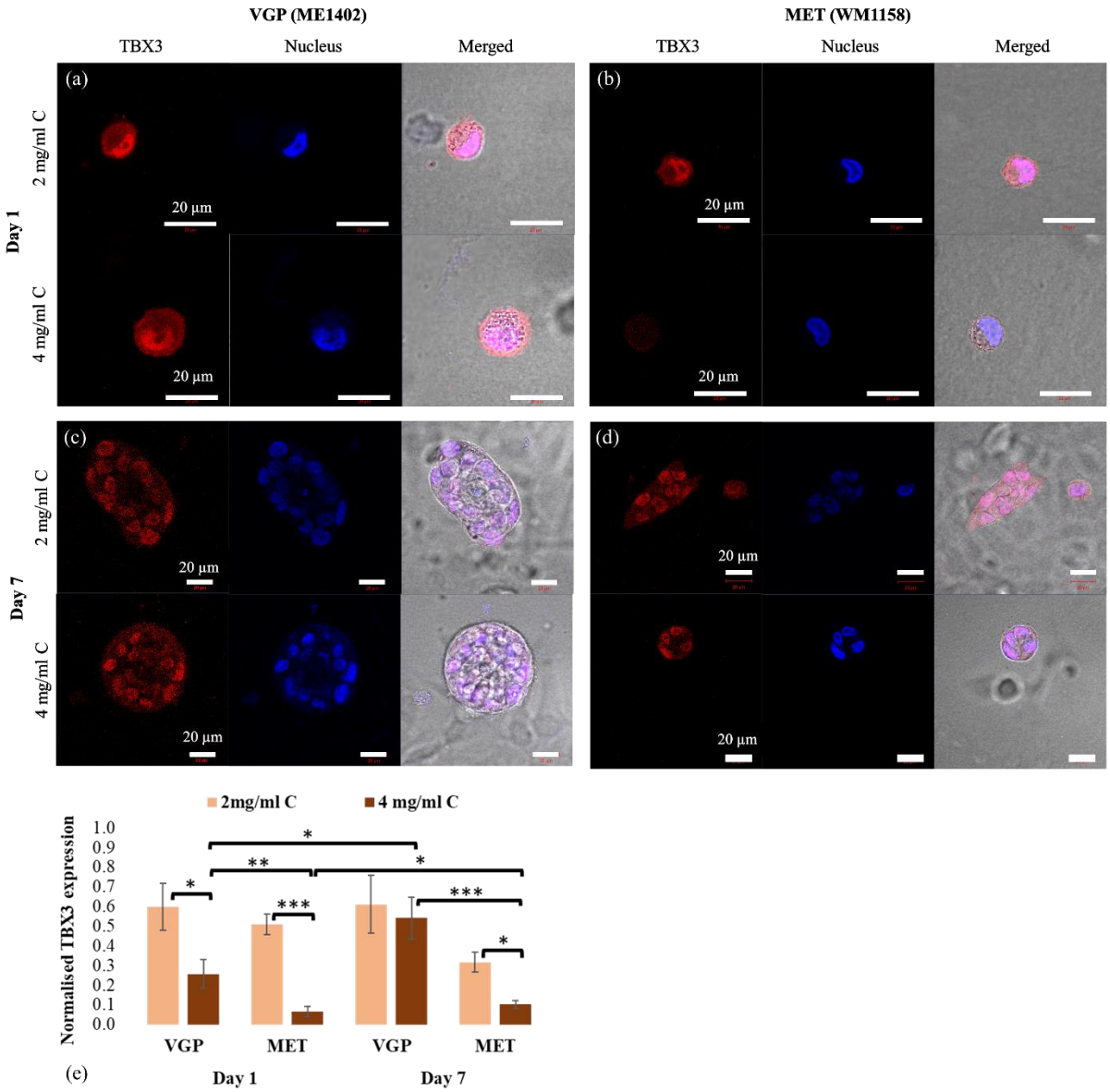

Figure 8: Fluorescent confocal images of TBX3 (red, left column), nucleus (blue, middle column) and merged TBX3 and nucleus superimposed on brightfield images (right column) for VGP and MET cells in 2 and 4 mg/ml collagen matrices after 24 hrs and 7 days (a – d). In merged TBX3 and nucleus fluorescence, pink colour indicates colocalization of TBX3 in the nucleus. (a, b): For isolated cells, TBX3 was expressed in the nuclei of VGP cells in 2 and 4 mg/ml collagen (a) and the nuclei of MET cells in 2 mg/ml collagen but not in 4 mg/ml collagen (b). (c, d): For cell clusters, TBX3 was expressed in the nuclei of VGP clusters in 2 and 4 mg/ml collagen (c) and nuclei of MET clusters in 2 and 4 mg/ml collagen (d). For each condition, sample size was N = 9 from n = 2 repeat experiments. Mid-2D focal plane, 63x

magnification, scale bar represents 20 µm.
*(e): Fluorescence of TBX3 normalized to nuclei. For isolated cells (Day 1), TBX3 was overexpressed in VGP and MET cells in 2 mg/ml collagen but decreased with increased collagen concentration. In 4 mg/ml collagen, TBX3 was expressed in isolated VGP cells but absent in MET cells. For cell clusters (Day 7), TBX3 in VGP was equally overexpressed in 2 and 4 mg/ml collagen. In MET clusters, TBX3 was expressed but lower in 4 mg/ml than 2 mg/ml collagen. (Statistical analyses were performed on the logarithmic transformation of normalized TBX3 data since untransformed data were not normally distributed; *** $p < .001$, ** $p < .005$ and * $p < .05$.)*

3.4.1. TBX3 in isolated cells was overexpressed in soft but not in stiff matrices

TBX3 was equally overexpressed in isolated VGP and MET cells in 2 mg/ml collagen ($p = .987$) (Figure 8e, Day 1). Compared to 2 mg/ml collagen, in 4 mg/ml collagen cellular TBX3 levels decreased by 57% ($p = .007$) for VGP and by 87% ($p < .001$) for MET cells. Notably, TBX3 was still detectable and present in VGP cells but nearly disappeared in MET cells in 4 mg/ml collagen.

3.4.2. TBX3 decreased with increased collagen concentration in MET but not VGP cell clusters

In cell clusters, TBX3 levels for MET were 48% lower than for VGP in 2 mg/ml collagen ($p = .344$, non-significant) and 81% lower than for VGP in 4 mg/ml collagen ($p < .001$) (Figure 8e, Day 7). TBX3 of MET clusters was 68% lower in 4 mg/ml than in 2 mg/ml collagen ($p = .006$) whereas TBX3 in VGP clusters was equally overexpressed in 2 and 4 mg/ml collagen ($p = .877$).

3.4.3. TBX3 increased during cluster formation in stiff but not soft matrices

TBX3 levels during VGP cluster formation (i.e. transition from isolated cells at Day 1 to cell clusters at Day 7) increased for 4 mg/ml collagen ($p =.028$) but did not change for 2 mg/ml collagen ($p =.731$) (Figure 8e). For MET cluster formation, TBX3 levels increased in 4 mg/ml collagen ($p = .032$) and decreased in 2 mg/ml collagen ($p = .201$, non-significant).

4. Discussion

We quantified and compared *in vitro* the morphology, intracellular mechanics and TBX3 expression in VGP and MET melanoma cells in isolation and cell aggregates following cluster formation over 10 days in 3D collagen matrices of two different rigidities.

4.1. Isolated cells

Compared to VGP cells, MET cells exhibited smaller volume and mitochondrial fluctuations but higher stiffness in soft and stiff 3D collagen matrices. This reflects evolutionary changes associated with melanoma disease progression. Regulation of cell volume has important biomechanical and biochemical implications. For example, reports have shown that reduced cell volume increases cell stiffness [55] and molecular crowding [56], hindering protein mobility and ultimately slowing several biochemical cascades. Importantly, we observed increased stiffness of melanoma cells in the more advanced MET disease stage than in the VGP stage. This contrasts several studies that report decreased stiffness with melanoma disease progression [57-59]. However, these studies did not consider the effect of the change in cell volume. Few studies have reported increased stiffness with increased metastatic potential in prostate [60, 61] and melanoma cancers [62].

It is important to note that VGP cells formed clusters, whereas MET cells predominantly invaded the 3D collagen matrices in isolation. It is recognized that the size and deformability of cancer cells may facilitate penetration through several barriers for secondary colonization [57]. However, VGP cells are yet to penetrate thick layers of skin and need mechanical reinforcement to do so [63]. It is proposed that the deformability of the large VGP cells is insufficient to allow isolated cells to invade the dermis efficiently. Instead, large cluster formation may serve as a more efficient alternative to invade the surrounding tissue than single-cell invasion.

Our results showed TBX3 overexpression in isolated VGP and MET cells in soft matrices. As previously mentioned, VGP cells quickly formed cell clusters, whereas MET cells mostly remained as isolated cells over time. Considering that TBX3 promotes tumour formation and metastasis [43], it is suggested that overexpressed TBX3 promotes migration and cluster formation in isolated VGP cells and migration but not cluster formation in MET cells.

A polyclonal antibody was used for TBX3 staining since TBX3 has previously been identified in the cytoplasm of cancer cells and it is thought that in addition to functioning as a transcription factor in the nucleus, it may have additional roles in the cytoplasm. A monoclonal antibody may have provided better staining if it is assumed that the cytoplasmic staining is non-specific.

Compared to the overexpressed intracellular TBX3 levels in soft matrices, TBX3 content was 2.3-fold lower in VGP cells and absent in MET cells in the stiff collagen matrix. These

results indicate that TBX3 is, in part, governed by the cell's mechanical interaction with its environment and the crucial signalling molecules [43]. Specifically, it is proposed that increased matrix rigidity increases actomyosin contractility, which in turn stimulates signalling molecules that have overlapping functions in cytoskeletal remodelling and the PI3K/AKT signalling pathway. Actomyosin contractility is primarily mediated by Rho GTPases, such as RhoA, Rac1 and Cdc42 [64]. Interestingly, it has been reported that Cdc42 activity decreases with increased collagen matrix rigidity [65] and that upregulation of the PI3K/AKT pathway correlates with decreased Cdc42 levels [66].

Cell stiffness increased for isolated MET cells but did not change for VGP cells with increased matrix rigidity. Recent studies have shown that increased matrix rigidity through increased collagen concentration contributes to decreased cell stiffness of isolated prostate [67] and breast cancer cells [44] in 3D environments. However, using cell lines from various stages of breast, colon, and pancreas cancers, Wullkopf, West, Leijnse, Cox, Madsen, Oddershede and Erler [18] showed that the cell stiffness of early-stage cancer cells was consistently unaffected by changes in matrix rigidity. In contrast, the cell stiffness of highly metastatic cells either increased or decreased, even within the same cancer type. For example, the cell stiffness of metastatic breast cancer MDA-MB-231 cells increased, whereas the stiffness of 4T1 metastatic breast cancer cells decreased with increased matrix rigidity [18].

The VGP cells' inability and the MET cells' ability to adjust their intracellular biomechanics in response to external cues agree in part with the results of Wullkopf, West, Leijnse, Cox, Madsen, Oddershede and Erler [18]. However, it is essential to note that the dissimilarity of VGP and MET cells in adjusting their mechanical properties may be rooted in the functional interaction between cell volume and the extracellular environment. In soft matrices, VGP cells were approximately double the size of MET cells. Accordingly, increased matrix rigidity condensed the volume of large VGP and small MET cells by 11.4 and 5.9%, respectively. Due to the large size, the VGP cells' compression may not immediately affect intracellular traffic, mitochondrial fluctuations, and cell stiffness. In contrast, intracellular traffic was innately confined in small MET cells in soft matrices. Condensation of MET cell size through increased matrix rigidity further compromised intracellular traffic.

4.2. Cluster formation and cell clusters

The onset of cluster formation for VGP cells was associated with changes in intracellular mechanical properties in rigid matrices but not in compliant matrices. In the soft collagen

matrices, the mitochondrial fluctuations and cell stiffness of VGP cell clusters (Day 7) were the same as that of isolated cells (Day 1). This steadiness of the intracellular properties suggests that VGP cells were innately endowed with suitable mechanical properties to form clusters in soft matrices. Cluster formation appeared as an automatic cell fate of VGP cells.

The similarity of TBX3 levels in isolated VGP cells and VGP cell clusters supports the innate endowment of VGP cells with essential internal machinery for cluster formation. Based on the established role of TBX3 in promoting tumour formation and metastasis [43], we propose that TBX3 overexpression in VGP cell clusters was imperative to mediate their collective migratory modes and the merging with adjacent clusters (see Figure 3). Further, VGP clusters in soft and stiff matrices were similar in cluster size (although different in shape) and, more importantly, in TBX3 expression. Remarkably, Li, Wang, Duan, Shi, Li, Zhang and Ren [68] demonstrated a strong correlation between TBX3 expression and tumour size.

Our findings of the increase of mitochondrial fluctuations and cell stiffness during VGP cluster formation, i.e. compared to isolated cells, are substantiated by previous studies. Mih, Marinkovic, Liu, Sharif and Tschumperlin [69] showed that increased matrix rigidity fosters increased proliferative conditions for the cell, and Cheng, Zielonka, McAllister, Tsai, Dwinell and Kalyanaraman [70] associated increased proliferation with increased mitochondrial activity.

In stiff matrices, VGP and MET cell clusters exhibited increased TBX3 expression compared to low and absent TBX3 expression, respectively, in isolated VGP and MET cells. Thus, increased expression demonstrates that TBX3 is indispensable during cluster formation in stiff environments.

It is also suggested that TBX3 enhances cluster formation through cell proliferation in stiff environments, considering that these environments facilitate an increased proliferative activity of cells [69]. Previous studies have argued that TBX3 promotes cell migration but impedes proliferation in pancreatic ductal adenocarcinomas, melanoma and breast cancers in 2D *in vitro* and in *in vivo* animal environments [71]. However, 2D *in vitro* conditions have limited physiological relevance [44]. Cells exhibit excessive proliferation and cell spreading in 2D compared to 3D environments, stemming from upregulated biochemical signalling that coordinate cell cycling and cell metabolism [4]. *In vivo* animal models better represent human physiological conditions [44] but pose challenges for the controlled variation of matrix rigidity and differentiation of metastatic dissemination mode [45].

Advanced melanoma metastasizes to several organs in the body, including lung, liver, brain and bone, with different environmental stiffnesses. Our finding that the intracellular stiffness changed during cluster formation in stiff but not in soft matrices suggests that soft matrices provide a more favourable environment for cluster growth. Interestingly, this aligns with clinical and biopsy reports indicating that lungs with soft tissue are often the first and the most common distant melanoma metastasis target [72]. Differences in TBX3 expression in melanoma cells in 3D environments of different stiffness observed in this study may have important implications for developing therapeutic approaches. Melanoma therapies that inhibit TBX3 overexpression may be effective in soft lung tissue but prove ineffective in stiff bone tissue. The change of intracellular stiffness and TBX3 expression in melanoma cells during cluster formation in differently stiff environments demonstrate the need to consider mechanical and molecular biomarkers of cancer malignancy in combination in a tissue-specific context.

In the current study, collagen concentration was used as a proxy for the stiffness of the collagen matrix. This approach has limitations, and it will be beneficial in future studies to quantify the matrix stiffness associated with different collagen concentrations to determine the alignment with physiological conditions. Collagen concentration also affects the matrix's microarchitecture, which can vastly alter cell behaviour independent of matrix stiffness. Future approaches should, therefore, incorporate the impact of collagen architecture, as well as the degradation of the collagen matrix affecting the microarchitecture over time, on cell behaviour. Future studies should also investigate the expression of TBX3 under different biomechanical conditions.

5. Conclusions

Advanced melanoma metastasises to several organs in the body, including lung, liver, brain and bone, each having a unique environmental stiffness. Our finding that the intracellular stiffness changed during VGP and MET cluster formation in stiff but not in soft matrices suggests that soft matrices provide a more favourable environment for tumour growth. Interestingly, this aligns with clinical and biopsy reports indicating that lungs with soft tissue are often the first and the most common distant melanoma metastasis target [72]. Differences in TBX3 expression in melanoma cells in 3D environments of different stiffness observed in this study may have important implications for developing therapeutic approaches.

Melanoma therapies based on inhibiting TBX3 overexpression may be effective in soft lung tissue but prove ineffective in stiff bone tissue. The change of intracellular stiffness and TBX3 expression in melanoma cells during tumour formation in differently stiff environments demonstrate the need to consider mechanical and molecular biomarkers of cancer malignancy in combination in a tissue-specific context.

Data

Data supporting the results presented in this article are available on the University of Cape Town's institutional data repository (ZivaHub) under http://doi.org/10.25375/uct.14254394 as Higgins G, Higgins F, Peres J, M. Lang D, Abdalrahman T, H. Zaman M, Prince S, Franz T. Data for "Intracellular stiffness, mitochondrial activity and TBX3 expression jointly dictate the spreading mode of melanoma cells in 3D environments". ZivaHub, 2022, DOI: 10.25375/uct.14254394

Acknowledgements

We acknowledge the technical assistance of Mrs Susan Cooper of the Confocal and Light Microscope Imaging Facility of the University of Cape Town. The microscope used in this work was purchased with funds from the Wellcome Trust (grant number 108473/Z/15/Z) and the National Research Foundation of South Africa (grant number UID93197). Ms Anneli Hardy from the Statistical Consulting Service at the Department of Statistical Sciences, University of Cape Town, is acknowledged for conducting the regression model analysis.

Declaration of interest

None.

Funding sources

This study was supported financially by the National Research Foundation of South Africa (grant number IFR14011761118 to TF and grant number SRUG190306422357 to SP), the South African Medical Research Council (TF and SP), the Cancer Association of South Africa (SP), and the University of Cape Town (TF and SP). The funders had no role in study design, data collection and analysis, decision to publish, or preparation of the manuscript. Any opinion, findings and conclusions or recommendations expressed in this publication are

those of the authors and do not necessarily represent the official views of the funding agencies.

References

[1] D.B. Agus, J.F. Alexander, W. Arap, S. Ashili, J.E. Aslan, R.H. Austin, V. Backman, K.J. Bethel, R. Bonneau, W.-C. Chen, C. Chen-Tanyolac, N.C. Choi, S.A. Curley, M. Dallas, D. Damania, P.C.W. Davies, P. Decuzzi, L. Dickinson, L. Estevez-Salmeron, V. Estrella, M. Ferrari, C. Fischbach, J. Foo, S.I. Fraley, C. Frantz, A. Fuhrmann, P. Gascard, R.A. Gatenby, Y. Geng, S. Gerecht, R.J. Gillies, B. Godin, W.M. Grady, A. Greenfield, C. Hemphill, B.L. Hempstead, A. Hielscher, W.D. Hillis, E.C. Holland, A. Ibrahim-Hashim, T. Jacks, R.H. Johnson, A. Joo, J.E. Katz, L. Kelbauskas, C. Kesselman, M.R. King, K. Konstantopoulos, C.M. Kraning-Rush, P. Kuhn, K. Kung, B. Kwee, J.N. Lakins, G. Lambert, D. Liao, J.D. Licht, J.T. Liphardt, L. Liu, M.C. Lloyd, A. Lyubimova, P. Mallick, J. Marko, O.J.T. McCarty, D.R. Meldrum, F. Michor, S.M. Mumenthaler, V. Nandakumar, T.V. O'Halloran, S. Oh, R. Pasqualini, M.J. Paszek, K.G. Philips, C.S. Poultney, K. Rana, C.A. Reinhart-King, R. Ros, G.L. Semenza, P. Senechal, M.L. Shuler, S. Srinivasan, J.R. Staunton, Y. Stypula, H. Subramanian, T.D. Tlsty, G.W. Tormoen, Y. Tseng, A. van Oudenaarden, S.S. Verbridge, J.C. Wan, V.M. Weaver, J. Widom, C. Will, D. Wirtz, J. Wojtkowiak, P.-H. Wu, A physical sciences network characterization of non-tumorigenic and metastatic cells, Sci Rep 3 (2013) 1449.

[2] M. Mak, R.D. Kamm, M.H. Zaman, Impact of dimensionality and network disruption on microrheology of cancer cells in 3D environments, PLoS Comput Biol 10(11) (2014) e1003959.

[3] M.E. Fernandez-Sanchez, T. Brunet, J.C. Roper, E. Farge, Mechanotransduction's impact on animal development, evolution, and tumorigenesis, Annu Rev Cell Dev Biol 31 (2015) 373-97.

[4] D.S. Reynolds, K.M. Tevis, W.A. Blessing, Y.L. Colson, M.H. Zaman, M.W. Grinstaff, Breast cancer spheroids reveal a differential cancer stem cell response to chemotherapeutic treatment, Sci Rep 7(1) (2017) 10382.

[5] C.T. Mierke, D. Rosel, B. Fabry, J. Brabek, Contractile forces in tumor cell migration, Eur. J. Cell Biol. 87(8-9) (2008) 669-76.

[6] C.M. Kraning-Rush, J.P. Califano, C.A. Reinhart-King, Cellular traction stresses increase with increasing metastatic potential, PLoS One 7(2) (2012) e32572.

[7] V. Peschetola, V.M. Laurent, A. Duperray, R. Michel, D. Ambrosi, L. Preziosi, C. Verdier, Time-dependent traction force microscopy for cancer cells as a measure of invasiveness, Cytoskeleton (Hoboken) 70(4) (2013) 201-14.

[8] M. Guo, A.J. Ehrlicher, S. Mahammad, H. Fabich, M.H. Jensen, J.R. Moore, J.J. Fredberg, R.D. Goldman, D.A. Weitz, The role of vimentin intermediate filaments in cortical and cytoplasmic mechanics, Biophys J 105(7) (2013) 1562-8.

[9] T.W. Remmerbach, F. Wottawah, J. Dietrich, B. Lincoln, C. Wittekind, J. Guck, Oral cancer diagnosis by mechanical phenotyping, Cancer Res 69(5) (2009) 1728-32.

[10] D. Jaiswal, N. Cowley, Z. Bian, G. Zheng, K.P. Claffey, K. Hoshino, Stiffness analysis of 3D spheroids using microtweezers, PLoS One 12(11) (2017) e0188346.

[11] A.V. Taubenberger, S. Girardo, N. Traber, E. Fischer-Friedrich, M. Krater, K. Wagner, T. Kurth, I. Richter, B. Haller, M. Binner, D. Hahn, U. Freudenberg, C. Werner, J. Guck, 3D microenvironment stiffness regulates tumor spheroid growth and mechanics via p21 and ROCK, Adv Biosyst 3(9) (2019) e1900128.

[12] A. Blumlein, N. Williams, J.J. McManus, The mechanical properties of individual cell spheroids, Sci Rep 7(1) (2017) 7346.

[13] Y. Li, M.J. Fanous, K.A. Kilian, G. Popescu, Quantitative phase imaging reveals matrix stiffness-dependent growth and migration of cancer cells, Sci Rep 9(1) (2019) 248.

[14] D.T. Butcher, T. Alliston, V.M. Weaver, A tense situation: forcing tumour progression, Nat Rev Cancer 9(2) (2009) 108-22.

[15] J. Plou, Y. Juste-Lanas, V. Olivares, C. Del Amo, C. Borau, J.M. Garcia-Aznar, From individual to collective 3D cancer dissemination: roles of collagen concentration and TGF-beta, Sci Rep 8(1) (2018) 12723.

[16] J. Sapudom, S. Rubner, S. Martin, T. Kurth, S. Riedel, C.T. Mierke, T. Pompe, The phenotype of cancer cell invasion controlled by fibril diameter and pore size of 3D collagen networks, Biomaterials 52 (2015) 367-75.

[17] J.T. Erler, V.M. Weaver, Three-dimensional context regulation of metastasis, Clin Exp Metastasis 26(1) (2009) 35-49.

[18] L. Wullkopf, A.V. West, N. Leijnse, T.R. Cox, C.D. Madsen, L.B. Oddershede, J.T. Erler, Cancer cells' ability to mechanically adjust to extracellular matrix stiffness correlates with their invasive potential, Mol Biol Cell 29(20) (2018) 2378-2385.

[19] T.R. Cox, J.T. Erler, Remodeling and homeostasis of the extracellular matrix: implications for fibrotic diseases and cancer, Dis Model Mech 4(2) (2011) 165-78.

[20] P. Lu, V.M. Weaver, Z. Werb, The extracellular matrix: a dynamic niche in cancer progression, J Cell Biol 196(4) (2012) 395-406.

[21] P.P. Provenzano, D.R. Inman, K.W. Eliceiri, H.E. Beggs, P.J. Keely, Mammary epithelial-specific disruption of focal adhesion kinase retards tumor formation and metastasis in a transgenic mouse model of human breast cancer, Am J Pathol 173(5) (2008) 1551-65.

[22] L.C. van Kempen, J. Rijntjes, I. Mamor-Cornelissen, S. Vincent-Naulleau, M.J. Gerritsen, D.J. Ruiter, M.C. van Dijk, C. Geffrotin, G.N. van Muijen, Type I collagen expression contributes to angiogenesis and the development of deeply invasive cutaneous melanoma, Int J Cancer 122(5) (2008) 1019-29.

[23] P.P. Provenzano, P.J. Keely, Mechanical signaling through the cytoskeleton regulates cell proliferation by coordinated focal adhesion and Rho GTPase signaling, J Cell Sci 124(Pt 8) (2011) 1195-205.

[24] S.T. Sit, E. Manser, Rho GTPases and their role in organizing the actin cytoskeleton, J Cell Sci 124(Pt 5) (2011) 679-83.

[25] J. Zhong, Y. Yang, L. Liao, C. Zhang, Matrix stiffness-regulated cellular functions under different dimensionalities, Biomater Sci 8(10) (2020) 2734-2755.

[26] N.M.E. Ayad, S. Kaushik, V.M. Weaver, Tissue mechanics, an important regulator of development and disease, Philos Trans R Soc Lond B Biol Sci 374(1779) (2019) 20180215.

[27] S. Dupont, L. Morsut, M. Aragona, E. Enzo, S. Giulitti, M. Cordenonsi, F. Zanconato, J. Le Digabel, M. Forcato, S. Bicciato, N. Elvassore, S. Piccolo, Role of YAP/TAZ in mechanotransduction, Nature 474(7350) (2011) 179-83.

[28] A.D. Doyle, N. Carvajal, A. Jin, K. Matsumoto, K.M. Yamada, Local 3D matrix microenvironment regulates cell migration through spatiotemporal dynamics of contractility-dependent adhesions, Nat Commun 6 (2015) 8720.

[29] M. Krause, K. Wolf, Cancer cell migration in 3D tissue: negotiating space by proteolysis and nuclear deformability, Cell Adh Migr 9(5) (2015) 357-66.

[30] D. Lachowski, E. Cortes, D. Pink, A. Chronopoulos, S.A. Karim, P.M. J, A.E. Del Rio Hernandez, Substrate rigidity controls activation and durotaxis in pancreatic stellate cells, Sci Rep 7(1) (2017) 2506.

[31] M.J. Paszek, N. Zahir, K.R. Johnson, J.N. Lakins, G.I. Rozenberg, A. Gefen, C.A. Reinhart-King, S.S. Margulies, M. Dembo, D. Boettiger, D.A. Hammer, V.M. Weaver, Tensional homeostasis and the malignant phenotype, Cancer Cell 8(3) (2005) 241-54.

[32] J. Kapeleris, H. Zou, Y. Qi, Y. Gu, J. Li, J. Schoning, M.J. Monteiro, W. Gu, Cancer stemness contributes to cluster formation of colon cancer cells and high metastatic potentials, Clin Exp Pharmacol Physiol 47(5) (2020) 838-847.

[33] D.A. Close, D.P. Camarco, F. Shan, S.J. Kochanek, P.A. Johnston, The Generation of Three-Dimensional Head and Neck Cancer Models for Drug Discovery in 384-Well Ultra-Low Attachment Microplates, Methods Mol Biol 1683 (2018) 355-369.

[34] M. Singh, D.A. Close, S. Mukundan, P.A. Johnston, S. Sant, Production of Uniform 3D Microtumors in Hydrogel Microwell Arrays for Measurement of Viability, Morphology, and Signaling Pathway Activation, Assay Drug Dev Technol 13(9) (2015) 570-83.

[35] J.E. Ekert, K. Johnson, B. Strake, J. Pardinas, S. Jarantow, R. Perkinson, D.C. Colter, Three-dimensional lung tumor microenvironment modulates therapeutic compound responsiveness in vitro--implication for drug development, PLoS One 9(3) (2014) e92248.

[36] C.J. Lovitt, T.B. Shelper, V.M. Avery, Miniaturized three-dimensional cancer model for drug evaluation, Assay Drug Dev Technol 11(7) (2013) 435-48.

[37] H.P. Naber, E. Wiercinska, E. Pardali, T. van Laar, E. Nirmala, A. Sundqvist, H. van Dam, G. van der Horst, G. van der Pluijm, B. Heckmann, E.H. Danen, P. Ten Dijke, BMP-7

inhibits TGF-beta-induced invasion of breast cancer cells through inhibition of integrin beta(3) expression, Cell Oncol (Dordr) 35(1) (2012) 19-28.

[38] H.P. Naber, E. Wiercinska, P. Ten Dijke, T. van Laar, Spheroid assay to measure TGF-beta-induced invasion, J Vis Exp (57) (2011) e3337.

[39] S. Lam, E. Wiercinska, A.F. Teunisse, K. Lodder, P. ten Dijke, A.G. Jochemsen, Wild-type p53 inhibits pro-invasive properties of TGF-beta3 in breast cancer, in part through regulation of EPHB2, a new TGF-beta target gene, Breast Cancer Res Treat 148(1) (2014) 7-18.

[40] J. Peres, S. Mowla, S. Prince, The T-box transcription factor, TBX3, is a key substrate of AKT3 in melanomagenesis, Oncotarget 6(3) (2015) 1821-1833.

[41] J. Peres, E. Davis, S. Mowla, D.C. Bennett, J.A. Li, S. Wansleben, S. Prince, The highly homologous T-Box transcription factors, TBX2 and TBX3, have distinct roles in the oncogenic process, Genes and Cancer 1(3) (2010) 272-282.

[42] J. Peres, S. Prince, The T-box transcription factor, TBX3, is sufficient to promote melanoma formation and invasion, Mol. Cancer 12(1) (2013).

[43] S.F. Khan, V. Damerell, R. Omar, M. Du Toit, M. Khan, H.M. Maranyane, M. Mlaza, J. Bleloch, C. Bellis, B.D.B. Sahm, J. Peres, K.N. ArulJothi, S. Prince, The roles and regulation of TBX3 in development and disease, Gene 726 (2020) 144223.

[44] J.E. Kim, D.S. Reynolds, M.H. Zaman, M. Mak, Characterization of the mechanical properties of cancer cells in 3D matrices in response to collagen concentration and cytoskeletal inhibitors, Integr Biol (Camb) 10(4) (2018) 232-241.

[45] M. Cavo, M. Fato, L. Penuela, F. Beltrame, R. Raiteri, S. Scaglione, Microenvironment complexity and matrix stiffness regulate breast cancer cell activity in a 3D in vitro model, Sci Rep 6 (2016) 35367.

[46] J. Schindelin, I. Arganda-Carreras, E. Frise, V. Kaynig, M. Longair, T. Pietzsch, S. Preibisch, C. Rueden, S. Saalfeld, B. Schmid, J.Y. Tinevez, D.J. White, V. Hartenstein, K. Eliceiri, P. Tomancak, A. Cardona, Fiji: an open-source platform for biological-image analysis, Nat Methods 9(7) (2012) 676-82.

[47] J.Y. Tinevez, N. Perry, J. Schindelin, G.M. Hoopes, G.D. Reynolds, E. Laplantine, S.Y. Bednarek, S.L. Shorte, K.W. Eliceiri, TrackMate: An open and extensible platform for single-particle tracking, Methods 115 (2017) 80-90.

[48] N. Tarantino, J.Y. Tinevez, E.F. Crowell, B. Boisson, R. Henriques, M. Mhlanga, F. Agou, A. Israel, E. Laplantine, TNF and IL-1 exhibit distinct ubiquitin requirements for inducing NEMO-IKK supramolecular structures, J Cell Biol 204(2) (2014) 231-45.

[49] V.V. Artym, K. Matsumoto, Imaging cells in three-dimensional collagen matrix, Curr Protoc Cell Biol Chapter 10 (2010) Unit 10 18 1-20.

[50] O. Gavet, J. Pines, Progressive activation of CyclinB1-Cdk1 coordinates entry to mitosis, Dev Cell 18(4) (2010) 533-43.

[51] P. Chugh, E.K. Paluch, The actin cortex at a glance, J Cell Sci 131(14) (2018).

[52] M. Guo, A.J. Ehrlicher, M.H. Jensen, M. Renz, J.R. Moore, R.D. Goldman, J. Lippincott-Schwartz, F.C. Mackintosh, D.A. Weitz, Probing the stochastic, motor-driven properties of the cytoplasm using force spectrum microscopy, Cell 158(4) (2014) 822-832.

[53] T.G. Mason, K. Ganesan, J.H. van Zanten, D. Wirtz, S.C. Kuo, Particle Tracking Microrheology of Complex Fluids, Phys. Rev. Lett. 79(17) (1997) 3282-3285.

[54] P.P. Kumar, S. Franklin, U. Emechebe, H. Hu, B. Moore, C. Lehman, M. Yandell, A.M. Moon, TBX3 regulates splicing in vivo: a novel molecular mechanism for Ulnar-mammary syndrome, PLoS Genet 10(3) (2014) e1004247.

[55] M. Guo, A.F. Pegoraro, A. Mao, E.H. Zhou, P.R. Arany, Y. Han, D.T. Burnette, M.H. Jensen, K.E. Kasza, J.R. Moore, F.C. Mackintosh, J.J. Fredberg, D.J. Mooney, J. Lippincott-Schwartz, D.A. Weitz, Cell volume change through water efflux impacts cell stiffness and stem cell fate, Proc Natl Acad Sci U S A 114(41) (2017) E8618-E8627.

[56] A. Miermont, F. Waharte, S. Hu, M.N. McClean, S. Bottani, S. Leon, P. Hersen, Severe osmotic compression triggers a slowdown of intracellular signaling, which can be explained by molecular crowding, Proc Natl Acad Sci U S A 110(14) (2013) 5725-30.

[57] M. Pachenari, S.M. Seyedpour, M. Janmaleki, S. Babazadeh Shayan, S. Taranejoo, H. Hosseinkhani, Mechanical properties of cancer cytoskeleton depend on actin filaments to

microtubules content: investigating different grades of colon cancer cell lines, J Biomech 47(2) (2014) 373-9.

[58] R. Omidvar, M. Tafazzoli-Shadpour, M.A. Shokrgozar, M. Rostami, Atomic force microscope-based single cell force spectroscopy of breast cancer cell lines: an approach for evaluating cellular invasion, J Biomech 47(13) (2014) 3373-9.

[59] W. Xu, R. Mezencev, B. Kim, L. Wang, J. McDonald, T. Sulchek, Cell stiffness is a biomarker of the metastatic potential of ovarian cancer cells, PLoS One 7(10) (2012) e46609.

[60] L. Bastatas, D. Martinez-Marin, J. Matthews, J. Hashem, Y.J. Lee, S. Sennoune, S. Filleur, R. Martinez-Zaguilan, S. Park, AFM nano-mechanics and calcium dynamics of prostate cancer cells with distinct metastatic potential, Biochim Biophys Acta 1820(7) (2012) 1111-20.

[61] E.C. Faria, N. Ma, E. Gazi, P. Gardner, M. Brown, N.W. Clarke, R.D. Snook, Measurement of elastic properties of prostate cancer cells using AFM, Analyst 133(11) (2008) 1498-500.

[62] G. Weder, M.C. Hendriks-Balk, R. Smajda, D. Rimoldi, M. Liley, H. Heinzelmann, A. Meister, A. Mariotti, Increased plasticity of the stiffness of melanoma cells correlates with their acquisition of metastatic properties, Nanomedicine 10(1) (2014) 141-8.

[63] J. Bobrowska, K. Awsiuk, J. Pabijan, P. Bobrowski, J. Lekki, K.M. Sowa, J. Rysz, A. Budkowski, M. Lekka, Biophysical and biochemical characteristics as complementary indicators of melanoma progression, Anal Chem 91(15) (2019) 9885-9892.

[64] N.S. Sipes, Y. Feng, F. Guo, H.O. Lee, F.S. Chou, J. Cheng, J. Mulloy, Y. Zheng, Cdc42 regulates extracellular matrix remodeling in three dimensions, J Biol Chem 286(42) (2011) 36469-77.

[65] S.J. Kim, Q. Wan, E. Cho, B. Han, M.C. Yoder, S.L. Voytik-Harbin, S. Na, Matrix rigidity regulates spatiotemporal dynamics of Cdc42 activity and vacuole formation kinetics of endothelial colony forming cells, Biochem Biophys Res Commun 443(4) (2014) 1280-5.

[66] L.E. Arias-Romero, J. Chernoff, Targeting Cdc42 in cancer, Expert Opin Ther Targets 17(11) (2013) 1263-73.

[67] E.L. Baker, R.T. Bonnecaze, M.H. Zaman, Extracellular matrix stiffness and architecture govern intracellular rheology in cancer, Biophys. J. 97(4) (2009) 1013-21.

[68] Z. Li, Y. Wang, S. Duan, Y. Shi, S. Li, X. Zhang, J. Ren, Expression of TBX3 in hepatocellular carcinoma and Its clinical implication, Med Sci Monit 24 (2018) 9324-9333.

[69] J.D. Mih, A. Marinkovic, F. Liu, A.S. Sharif, D.J. Tschumperlin, Matrix stiffness reverses the effect of actomyosin tension on cell proliferation, J Cell Sci 125(Pt 24) (2012) 5974-83.

[70] G. Cheng, J. Zielonka, D. McAllister, S. Tsai, M.B. Dwinell, B. Kalyanaraman, Profiling and targeting of cellular bioenergetics: inhibition of pancreatic cancer cell proliferation, Br J Cancer 111(1) (2014) 85-93.

[71] L. Perkhofer, K. Walter, I.G. Costa, M.C.R. Carrasco, T. Eiseler, S. Hafner, F. Genze, M. Zenke, W. Bergmann, A. Illing, M. Hohwieler, R. Köhntop, Q. Lin, K.-H. Holzmann, T. Seufferlein, M. Wagner, S. Liebau, P.C. Hermann, A. Kleger, M. Müller, Tbx3 fosters pancreatic cancer growth by increased angiogenesis and activin/nodal-dependent induction of stemness, Stem Cell Res. 17(2) (2016) 367-378.

[72] W.E. Damsky, L.E. Rosenbaum, M. Bosenberg, Decoding melanoma metastasis, Cancers 3(1) (2010) 126-63.